Stress-induced percolative core formation through a bridgmanite mantle

Lin Wang[1,*], Yingwei Fei[1]

[1] Earth and Planets Laboratory, Carnegie Institution for Science, U.S.

Corresponding author: Lin Wang (liwang@carnegiescience.edu)

Key Points:

- A new method of determining melt connectivity in silicate matrix was developed.
- Core-forming melts can form an interconnected network in a deformed bridgmanite matrix.
- Stress-induced percolation is a viable core formation mechanism in planets.
- The stranded melt in the Earth mantle left by core formation could explain its abundance of highly siderophile elements.

Abstract

Segregation of liquid metal from solid silicate is a necessary pathway for core formation in a large rocky planetary body during the planet growth. The mechanism and extent of such process have an important effect on the geophysical and geochemical properties of the planetary body. Percolative flow of core forming melts through a silicate mantle has been ruled out as a possible mechanism of core formation by hydrostatic annealing experiments at pressures less than 50 GPa. However, an evolving mantle is not static, but continually deforming. Here, using element migration in the melts as an effective indicator for melt connectivity, we conclusively demonstrated that iron alloy melts could form an interconnected network in a solid bridgmanite matrix under deformation, even at a small total strain of ~0.1. Depending on the grain size of bridgmanite, percolation as a core formation mechanism could leave mantle disequilibrium/equilibrium with the core. The result showed that ~0.4 vol.% liquid metal was trapped in the silicate mantle and the stranded metal alloy could explain the highly siderophile elements (HSE) chondritic abundance in the Earth's mantle without late veneer.

Plain Language Summary

We use element migration as an indicator of melt interconnection to demonstrate that core-forming melt can form an interconnected network in a bridgmanite matrix under deformation. The fast segregation velocity of melts in silicate makes the stress-induced percolation a feasible core formation mechanism. The melts left in the mantle after draining could explain the highly siderophile elements abundance in the Earth mantle.

1 Introduction

The mechanism of core formation plays an important role in determining the geochemical and geophysical properties of a planet. Migration of iron-rich core-forming melts to the center of the planet causes a depletion of siderophile elements in the mantle [*Jie Li and Agee*, 1996; *Rubie et al.*, 2007] and enrichment of light elements in the core [*J Li and Fei*, 2003]. Knowledge of core-formation mechanism is therefore essential to explain the siderophile elements abundance in the mantle and light elements budget in the core. The interaction of core-forming melts and mantle is also necessary to understand the large scale geophysical evolution in the planet [*Zhang et al.*, 2016]. Moreover, the mechanism of core-mantle segregation provides a constraint on the timing of core formation.

Core formation in the Earth includes settling iron alloy melts through a magma ocean and a solid silicate mantle [*Rubie et al.*, 2007; *Stevenson*, 1990]. The latter occurs when the descending alloy reaches the depth where the mantle has already solidified. Geochemical evidence suggested that the magma ocean in the Earth is not deep enough to cover the whole mantle [*Chabot et al.*, 2005]. Therefore, the segregation of core-forming melts and solid silicate is inevitable in the mantle. Under hydrostatic conditions, the efficiency of percolation as a mechanism in this process is controlled by the ratio of solid-melt interfacial energy (γ_{sl}) and solid-solid interfacial energy (γ_{ss}), which is reflected by the dihedral angle (θ) between two neighboring solid grains in contact with melt at a triple junction. For $\theta > 60°$, the ratio between γ_{sl} and γ_{ss} is so large that percolation is impossible unless the melts fraction exceeds a critical percolation threshold [*von Bargen and Waff*, 1986]. For $\theta < 60°$, the melts can form an interconnected network irrespective of melt fraction, through which complete drainage of melts by percolation is possible.

Previous hydrostatic annealing experiments have suggested that θ is higher than 60° for an iron alloy-silicate matrix system at pressures less than 50 GPa [*Minarik et al.*, 1996; *Shannon and Agee*, 1998; *Shi et al.*, 2013; *Takafuji et al.*, 2004; *Terasaki et al.*, 2007], ruling out percolation as an efficient core formation mechanism. However, there are certain limitations in such reasoning. First, the 60° dihedral angle as the criteria of melt interconnectivity can only be used in a matrix material with isotropic surface tension [*von Bargen and Waff*, 1986]. Such prerequisite is clearly not true for the mantle minerals due to their low crystal symmetry. More importantly, the solid silicate mantle may not be static but continually deforming due to the isostatic adjustment of silicate mantle after a large impact [*Tonks and Melosh*, 1992] and the heat induced mantle convection. The melts texture developed at hydrostatic conditions could have been continually perturbed by the convective straining of the matrix. This perturbation is not negligible especially for early Earth where mantle convection is vigorous [*Stevenson*, 1990]. Therefore, it is essential to study the percolation behavior under deformation with a more definitive criteria of the melt interconnectivity.

It has been proved that core forming melts can form an interconnected network by deformation in an olivine matrix [*Bruhn et al.*, 2000; *Groebner and Kohlstedt*, 2006; *Hustoft and Kohlstedt*, 2006], which has important implications for metal-silicate separation in small planets or asteroids. For large planets such as the Earth, bridgmanite, a strong dense silicate, is the dominant mantle phase, playing a critical role in metal-silicate separation after core-forming melts settles to the bottom of the magma ocean. It is virtually unknown about the effect of deformation on the percolation of iron alloy in a bridgmanite matrix because of lack of experimental data. Here, we provide the first look at stress-induced interconnectivity of core-forming melt in a bridgmanite matrix.

2 Materials and Methods

2.1 Synthesize of starting material:

Well sintered aggregate of 5% vol. Fe,S alloy (6% wt. S) and 95% vol. bridgmanite $(Mg_{0.9}Fe_{0.1})SiO_3$ were prepared using following procedures. A glass with desire bridgmanite composition was made from fusing a mixture of MgO, SiO_2 and Fe_2O_3 with prescribed ratio at 1923 K and room pressure followed by rapidly quenching into cold water using high temperature furnace at Bayerishes Geoinstitute, Univerisity Bayreuth, Germany (BGI). The glass was subsequently reduced in a gas mixture furnace (CO, CO2 gas) at 1523 K and an oxygen fugacity of one log unit above iron-wüsite buffer for 48 hours using gas mixing furnace at BGI. The synthesized enstatite powder was then mixed with Fe and FeS powder with prescribed ratio. The mixture was compressed to 25 GPa in the multi-anvil apparatus [*Bertka and Fei*, 1997] using an 8-3 assembly (Fig S1a). After heating to 1873 K, temperature was kept for 2 h for the transformation of enstatite to bridgmanite. Temperature was recorded by W95%Re5%–W74%Re26% thermocouple.

2.2 Deformation experiments:

Deformation experiments were conducted using the multi anvil apparatus at Carnegie. Fig. S1b shows a schematic of the cell assembly adopted in the present deformation experiments. The sintered starting material was shaped in to a cylinder with ~650μm diameter and 220 μm

thickness and was put into a Pt tube. Pt was used as an indicator of interconnection. If Fe-S alloy interconnects, Pt is expected to alloy with Fe and migration throughout the melts. If Fe-S remains isolated, Pt is expected to only alloy Fe at the sample-Pt tube interface. The sample and Pt tube were sandwiched by two 45°-cut crushable alumina and put into a MgO sleeve which is made from sintered MgO rod. A 50-μm thick Re foil was placed at the ends of each 45°-cut alumina piston to reduce the friction against the sideslip [*Tsujino et al.*, 2016]. A Re heater with 60μm thickness was used to generate high temperature. The temperature was extrapolated from the electric power on the basis of the calibrations from the synthesis experiments.

The specimens were first compressed to the 25 GPa (210 bar oil pressure) at room temperature, and then heated to 2100 K for 40 min to relax the deviatoric stress in the specimens and sinter crushable alumina piston. Then the oil pressure was increased to 250 bar in 2 h to deform the sample. The different compressibility of alumina and MgO capsule results in a deviatoric stress on the sample that leads to a shear of the sample. The total strain (ε) is estimated from the relative displacement of the two 45°-cut pistons (Fig S1c, S1d). In order to compare the deformed and undeformed samples directly under the same conditions, we also performed an experiment without deformation. For the undeformed sample, the specimen was compressed directly to 250 bar and heated to 2100 K for 2 hours. For all experiments, temperature was quenched by shutting off the power.

2.3 Data analysis

The recovered sample were mounted in epoxy resin and polished with SiC sand papers and diamond paste in sequence. The melt textures of the samples were observed with a field emission scanning electron microscope at Carnegie. The dihedral angles of Fe-S melts in the undeformed bridgmanite sample were measured in 2D cross sections. 121 melts pockets at triple junctions were measured. The Pt mapping of the samples and the composition analysis of Pt tube were made by energy dispersive spectroscopy. The 2D area of Pt-free melts in the deformed samples (see the results for details) was calculated using public software Image J. The area percentage of the melts was used as the volume percentage without further corrections.

3 Results

3.1 Melt textures after synthesis, annealing and deformation

The Raman spectrum shows that bridgmanite was successfully synthesized (Fig. S2). A secondary electron image (Fig. S2) of the sintered aggregation reveals that the Fe-S alloy was distributed evenly in the bridgmanite matrix. Some minor amount of Fe-rich (Mg,Fe)O was formed during the synthesis. This may be due to the oxidation of Fe during the experiments [*Frost and Langenhorst*, 2002].

The total strain of the deformed sample is ~0.1, estimated from the displacement of the pistons. The microstructures of the undeformed (annealing only) and deformed sample are shown in Fig 1a and Fig. 1b, respectively. The Fe-S melts in the undeformed sample exhibit isolated pockets, whose average apparent dihedral angle is 77° (Fig S3). The quenched metallic melts contain typical dendric Fe-S melt quench texture, indicating the iron alloy was fully melted at high temperature. The average composition of the melts is close to that of the starting metal alloy. All

melts pockets have a radius less than 15 μm. The distribution and topology of the metal melt are similar to those reported in previous studies without deformation [*Terasaki et al.*, 2007].

In contrast, the deformed sample, even with a total strain of ~ 0.1, shows alignment of the melt pockets. The aligned melts consist of elongated melts and isolated pockets and form an angle of 15°- 30° from the shear plane (Fig. 1b). Some pockets are elongated up to 45μm. Similar textures were reported in iron alloy deformed in an olivine matrix at low pressure [*Bruhn et al.*, 2000] but with much higher strain ($\varepsilon \sim 2.5$).

3.2 Pt distribution as an indicator of melt interconnectivity

The observed alignment of the melt under shear deformation provides a sign of melt interconnectivity. The definitive evidence for the melt interconnection by deformation comes from mapping the Pt distribution in the sample. Figures 2a and 2b show the metallic melt distribution through the entire undeformed and deformed samples, respectively, with Pt tubes shown on the edges. By Pt element mapping, we can clearly see that Pt element is only found locally in the melts near the Pt tube in the undeformed sample (Fig. 2c), whereas Pt element is found throughout the melts in the deformed sample (Fig. 2d). This demonstrates that an interconnected melt network is formed in the deformed sample, through which Pt migrate from the sample-tube boundary into the sample. Because the network is formed before Pt migrate into the melts, the composition change of the metallic melts due to Pt contamination does not change our conclusion about percolative behavior of Fe-S melts in the bridgmanite matrix. In addition to the Pt-bearing melts, 0.4 vol.% melts in the deformed sample are Pt free (Fig 1b).

Higher Fe content in the Pt tube holder in the deformed sample also supports the formation of the Fe-S melt network by deformation. The Fe contents in the Pt holder at the constant distance away from the holder-sample boundary were measured in the deformed and undeformed samples (Fig. S4). Three times higher Fe content was found in the deformed one. This is consistent with the an Fe-S network existing in the deformed sample, through which more amounts of Fe can migrate into the Pt holder.

Besides clear demonstration of forming an interconnected network, Pt content in the Fe-S melt pockets can also be used to trace melt channels. Two bands are identified from the apparently isolated melt pockets in the 2D section. (Fig. S5). Inside each band, individual melt pockets elongate in the same direction. Each band has similar brightness in a backscattered image, reflecting a similar Pt content. The observation indicates that these pockets form interconnected channels. These channels extend hundreds of micrometers. The Pt tracer method provides a simple visual image with detailed channel structure, complementary to previous time-consuming slicing-reconstruction [*von Bargen and Waff*, 1986] or 3D tomography [*Shi et al.*, 2013] method.

4 Discussion

4.1 Comparison with previous studies

Only a total strain of ~ 0.1 is needed for Fe-S melt interconnection in a bridgmanite matrix, which is much smaller than that needed in an olivine matrix [*Bruhn et al.*, 2000]. This may be due to the viscosity contrast between bridgmanite and melts is much higher than that between olivine and melts. Bridgmanite is much harder to deform than olivine [*Girard et al.*, 2015; *Groebner and Kohlstedt*, 2006]. Therefore, the melts in the bridgmanite matrix would like to accommodate more strain. This idea is supported by the fact that, although the total strain of the olivine study is much higher than that in this study, the extent of elongation of individual melt pockets (~40 μm) and the extension of melt channel (hundreds of micrometers) due to deformation in an olivine and a bridgmanite matrix are similar.

4.2 Scaling to the Earth conditions

Our experimental results on stress-induced melt connectivity can be used to understand melt percolation in the early Earth by assessing the controlling factors that influence the melt distribution. It is suggested that, at a given dihedral angle, the melt texture is controlled by the stain rate($\dot{\varepsilon}$) and the liquid pocket size(r) [*Walte et al.*, 2011]. At high $\dot{\varepsilon}$ and large r, stress controls the melt texture and melt could form an interconnected network. On the other hand, at low $\dot{\varepsilon}$ and small r, surface tension controls melt texture and melt tends to form isolated pocket. Therefore, the maximum r of unelongated melts pockets represent the upper boundary of the surface-tension-controlled regime while the minimum r of elongated melts pockets represents the lower boundary of the stress-controlled regime. The transition from stress-dominated to surface-tension dominated regime has a negative slope of $-1/n$ in the $\log(r)$-$\log(\dot{\varepsilon})$ plot, where n is controlled by the deformation mechanism [*Walte et al.*, 2011]. Our deformation experiment has r of the smallest elongated pocket ~ 1 μm and of the largest unelongated pocket ~ 6 μm, respectively. The $\dot{\varepsilon}$ in our experiment is ~ 10^{-5}. Assuming bridgmanite deformation is controlled by dislocation creep [*De Wit and Trampert*, 2015; *Ferreira et al.*, 2019] and it has the same n = 3.5 as olivine dislocation creep [*Hirth and Kohlstedt*, 2003], the regime where melt distribution is controlled by stress can be identified in the $\log(r)$-$\log(\dot{\varepsilon})$ plot (Fig. S6). Given the large diameter of melt pocket in meteorite [*Brearley*, 1998; *Mittlefehldt et al.*, 1998] and strain rate in the earth mantle (10^{-12}-10^{-14}) [*Walte et al.*, 2011], the melt texture in the real earth could fall in the stress-dominated regime. Actually, the strain rate of mantle in the early earth could have higher strain rate [*Stevenson*, 1990]. This further moves the melt texture in the natural condition in the stress-dominated regime (Fig. S6). Recent study [*Berg et al.*, 2017] even suggested that the deformation-aided melt segregation is independent of the strain rate at high pressure, implying that no scaling is needed to apply the experimental results to the natural environment. Therefore, the stress-induced percolation could occur during the metal-silicate segregation in the early Earth.

5 Implications

5.1 Estimation of segregation velocity

The segregation velocity (V_m) of a fluid through a porous matrix is expressed as [*Faul*, 1997; *McKenzie*, 1989]

$$V_m = \frac{k \Delta \rho g}{\varphi \mu} \qquad (1)$$

where k is permeability, $\Delta\rho$ is the density different between solid and liquid (3500kg/m^3), μ is the viscosity of melt, taken as 0.04 Pa·s [*Terasaki et al.*, 2001], φ is the melt fraction, g is the acceleration due to gravity. k can be expressed as [*Turcotte and Schubert*, 2002]

$$k = \frac{d^2 \varphi^n}{C} \qquad (2)$$

where d is grain size, C is a constant depending on the melt network geometry. Many studies have estimated the V_m of the core-forming melts in silicate [*Bagdassarov et al.*, 2009; *Berg et al.*, 2018; *Roberts et al.*, 2007; *Todd et al.*, 2016] and the exponent, n, ranges from 1-3.8 [*Faul*, 1997; *Roberts et al.*, 2007]. Accordingly, the estimated V_m varies by orders of magnitude. Here, due to the inconsistency of experimental data and lack of data on the V_m of core-forming melts in a bridgmanite matrix, we estimate the V_m using a theoretical solutions for melts segregation in a network of interconnected tubules (hereafter called tubules model), where $C = 72\pi$ and $n = 2$ and the experimental result for melts migration in olivine matrix [*Roberts et al.*, 2007] (hereafter called olivine-ref model), where $C = 250$ and $n = 3.6$.

Figure 3 shows the calculated V_m as a function of grain size and melt fraction. The grain size of bridgmanite is not well constrained and its estimation varies from ~20 μm to mm size [*Dannberg et al.*, 2017; *Solomatov et al.*, 2002; *Yamazaki et al.*, 1996]. However, even with the smallest estimation (~20 μm), V_m values is ~0.2 m/yr at melt fraction of 0.1 (Equ. 1, Equ. 2 and Fig. 3). It needs ~ 15 My to drain the melts through the Earth lower mantle. This time scale is within the 30 My duration of core formation based on the mantle Hf-W isotopic ratios [*Kleine et al.*, 2002]. Therefore, the stress-induced percolation is an effective mechanism for the Earth core formation.

5.2 Implication to grain size of bridgmanite and highly siderophile elements abundance in the lower mantle

Depending on the grain size of bridgmanite, the V_m values are good indicator if the mantle is in equilibrium/disequilibrium with the descending core forming melts. The descending melts change their composition with the surrounding mantle by diffusion. If V_m is so large that the diffusion distance in the solid (d_s) during the melts residence time is less than the average distance between the melt channels (d_m), mantle is in disequilibrium with the melts. Because d_m cannot be smaller than the grain size d, if $d > d_s$, mantle is definitely in disequilibrium with the melts. The blue curve in Fig. 3 shows the boundary between equilibrium and disequilibrium regions in both melt network models using a lower mantle thickness of 3000 km.

The siderophile elements abundance in the mantle and core suggested a disequilibrium between the Earth core and lower mantle [*Chabot et al.*, 2005]. Therefore, the lower limit of grain size of bridgmanite in the lower mantle can be constrained if the correct parameters in the formula of k (C and n in Equ. 2) are used, assuming percolation is the major mechanism for melt-silicate segregation. In the tubules model, a grain size of 300 μm is large enough for mantle-core disequilibrium with $\varphi = 0.1$. However, the grain size has to be larger than 800 μm to reach the same conclusion in the olivine-ref model. Further study on the V_m could better constrain the grain size of bridgmanite, which is an essential parameter for the lower mantle rheology.

The 0.4 vol.% Pt-free melts in the deformed sample indicates that those melt pockets were not connected to the interconnected melt network. The value could represent the upper limit of the stranded melts in the mantle after the melts in the melt channels were drained completely during core formation [*Groebner and Kohlstedt*, 2006] and further deformation to a large strain of mantle could reduce the amount of stranded melts [*Groebner and Kohlstedt*, 2006; *Hustoft and Kohlstedt*, 2006]. Because those stranded core melts have a chondritic ratio of highly siderophile elements (HSE), it could potentially explain the observed HSE abundance in the Earth mantle [*McDonough and Sun*, 1995] without invoking a late veneer scenario [*O'Neill*, 1991]. Assuming HSE abundance in the core forming melts is the same as that in the CI chondrite, 0.3 vol.% (0.7 wt.%) melts relative to the whole mantle are needed to explain the HSE abundance observed in the mantle. This is consistent with the 0.4 vol. % stranded melts in the lower mantle which is 70% vol. of the total silicate Earth.

5.3 Stress-induced percolation scenario for the core-formation in rocky planets

Stress-induced percolation could occur under different scenarios during the Earth core formation (Fig. 4). As the iron droplets in molten mantle silicate descend to the bottom of the magma ocean, they would accumulate as a ponded layer due to the high viscosity of the underlying bridgmanite layer until a critical thickness for Rayleigh-Taylor instability is reached [*Honda et al.*, 1993]. Due to mantle convection, the iron alloy could be trapped and form an interconnected network in the bridgmanite matrix and drain the melts from the pond to the proto-core. Once the ponded layer reaches the critical thickness, large diapirs of melt would form. The high stress caused by the diapir descending could also induce an interconnected melt network in the surrounding mantle [*Golabek et al.*, 2008]. In addition, any remaining core melt distributed on the grain scale left by the diapir would be subjected to the deformation and could be redistributed into a network for further descending. The fast descending velocity leaves the mantle in disequilibrium with the core forming melts. Although at greater depth (P>50 GPa) [*Shi et al.*, 2013] , pressure could reduce the dihedral angel of Fe-S less than 60^o in the bridgmanite matrix, deformation could enhance the permeability and the efficiency of core formation [*Hustoft and Kohlstedt*, 2006]. The stranded metallic melts could have moved upward and been oxidized in the Fe^{3+}-rich bridgmanite mantle [*Frost et al.*, 2004] by mantle convection, supplying the mantle a chondritic ratio of HSE abundance.

Finally, the described scenario is also applicable to the core formation in Mars. Mars is expected to have a bridgmanite layer above its core [*Bertka and Fei*, 1997]. Because the pressure at the core-mantle boundary in Mars is less than 50GPa, iron alloy cannot be interconnected without

deformation under these conditions, Therefore, under the Martian lower mantle conditions, the stress-induced interconnected network in the bridgmanite mantle is the only viable mechanism for metal percolation and could play an even more important role in Mars at the last stage of core formation.

Acknowledgments

We acknowledge N. Walte for the discussions of the manuscript. This research was supported by NASA grants to Y. Fei (80NSSC20K0337) and by the Carnegie fellowship.

References

Bagdassarov, N., G. Solferino, G. Golabek, and M. Schmidt (2009), Centrifuge assisted percolation of Fe–S melts in partially molten peridotite: time constraints for planetary core formation, *Earth and Planetary Science Letters*, *288*(1-2), 84-95.

Berg, M. T., G. D. Bromiley, Y. Le Godec, J. Philippe, M. Mezouar, J.-P. Perrillat, and N. J. Potts (2018), Rapid Core Formation in Terrestrial Planets by Percolative Flow: In-Situ Imaging of Metallic Melt Migration Under High Pressure/Temperature Conditions, *Frontiers in Earth Science*, *6*, 77.

Berg, M. T., G. D. Bromiley, I. B. Butler, M. Frost, R. Bradley, J. Carr, Y. Le Godec, L. G. Montési, W. Zhu, and K. Miller (2017), Deformation-aided segregation of Fe-S liquid from olivine under deep Earth conditions: Implications for core formation in the early solar system, *Physics of the Earth and Planetary Interiors*, *263*, 38-54.

Bertka, C. M., and Y. Fei (1997), Mineralogy of the Martian interior up to core−mantle boundary pressures, *Journal of Geophysical Research: Solid Earth*, *102*(B3), 5251-5264.

Brearley, A. J. a. J. R. H. (1998), Chondritic meteorites, *Planetary materials, Reviews in Mineralogy*, *36*.

Bruhn, D., N. Groebner, and D. L. Kohlstedt (2000), An interconnected network of core-forming melts produced by shear deformation, *Nature*, *403*(6772), 883-886.

Chabot, N. L., D. S. Draper, and C. B. Agee (2005), Conditions of core formation in the Earth: constraints from nickel and cobalt partitioning, *Geochimica et Cosmochimica Acta*, *69*(8), 2141-2151.

Dannberg, J., Z. Eilon, U. Faul, R. Gassmöller, P. Moulik, and R. Myhill (2017), The importance of grain size to mantle dynamics and seismological observations, *Geochemistry, Geophysics, Geosystems*, *18*(8), 3034-3061.

De Wit, R., and J. Trampert (2015), Robust constraints on average radial lower mantle anisotropy and consequences for composition and texture, *Earth and Planetary Science Letters*, *429*, 101-109.

Faul, U. H. (1997), Permeability of partially molten upper mantle rocks from experiments and percolation theory, *Journal of Geophysical Research: Solid Earth*, *102*(B5), 10299-10311.

Ferreira, A. M., M. Faccenda, W. Sturgeon, S.-J. Chang, and L. Schardong (2019), Ubiquitous lower-mantle anisotropy beneath subduction zones, *Nature Geoscience*, *12*(4), 301.

Frost, D. J., and F. Langenhorst (2002), The effect of Al2O3 on Fe–Mg partitioning between magnesiowüstite and magnesium silicate perovskite, *Earth and Planetary Science Letters*, *199*(1-2), 227-241.

Frost, D. J., C. Liebske, F. Langenhorst, C. A. McCammon, R. G. Trønnes, and D. C. Rubie (2004), Experimental evidence for the existence of iron-rich metal in the Earth's lower mantle, *Nature*, *428*(6981), 409.

Girard, J., G. Amulele, R. Farla, A. Mohiuddin, and S.-i. Karato (2015), Shear deformation of bridgmanite and magnesiowüstite aggregates at lower mantle conditions, *Science*, aad3113.

Golabek, G. J., H. Schmeling, and P. J. Tackley (2008), Earth's core formation aided by flow channelling instabilities induced by iron diapirs, *Earth and Planetary Science Letters*, *271*(1-4), 24-33.

Groebner, N., and D. L. Kohlstedt (2006), Deformation-induced metal melt networks in silicates: Implications for core–mantle interactions in planetary bodies, *Earth and Planetary Science Letters*, *245*(3-4), 571-580.

Hirth, G., and D. Kohlstedt (2003), Rheology of the Upper Mantle and the Mantle Wedge: A View from the Experimentalists, in *Inside the Subduction Factory*, edited, pp. 83-105, American Geophysical Union.

Holzapfel, C., D. C. Rubie, D. J. Frost, and F. Langenhorst (2005), Fe-Mg interdiffusion in (Mg, Fe) SiO3 perovskite and lower mantle reequilibration, *Science*, *309*(5741), 1707-1710.

Honda, R., H. Mizutani, and T. Yamamoto (1993), Numerical simulation of Earth's core formation, *Journal of Geophysical Research: Solid Earth*, *98*(B2), 2075-2089.

Hustoft, J. W., and D. L. Kohlstedt (2006), Metal−silicate segregation in deforming dunitic rocks, *Geochemistry, Geophysics, Geosystems*, *7*(2).
Kleine, T., C. Münker, K. Mezger, and H. Palme (2002), Rapid accretion and early core formation on asteroids and the terrestrial planets from Hf–W chronometry, *Nature*, *418*(6901), 952-955.
Li, J., and C. B. Agee (1996), Geochemistry of mantle–core differentiation at high pressure, *Nature*, *381*(6584), 686.
Li, J., and Y. Fei (2003), Experimental constraints on core composition, *TrGeo*, *2*, 568.
McDonough, W. F., and S.-S. Sun (1995), The composition of the Earth, *Chemical geology*, *120*(3-4), 223-253.
McKenzie, D. (1989), Some remarks on the movement of small melt fractions in the mantle, *Earth and planetary science letters*, *95*(1-2), 53-72.
Minarik, W. G., F. J. Ryerson, and E. B. Watson (1996), Textural entrapment of core-forming melts, *Science*, *272*(5261), 530.
Mittlefehldt, D. W., T. J. McCoy, C. A. Goodrich, and A. Kracher (1998), Non-chondritic meteorites from asteroidal bodies, *Reviews in Mineralogy and Geochemistry*.
O'Neill, H. S. C. (1991), The origin of the Moon and the early history of the Earth—A chemical model. Part 2: The Earth, *Geochimica et Cosmochimica Acta*, *55*(4), 1159-1172.
Roberts, J., J. Kinney, J. Siebert, and F. Ryerson (2007), Fe−Ni−S melt permeability in olivine: Implications for planetary core formation, *Geophysical Research Letters*, *34*(14).
Rubie, D. C., F. Nimmo, H. J. Melosh, and 2007. (2007), Formation of the Earth's core, *Treatise on Geophysics. : In: Stevenson, D. (Ed.), Evolution of the Earth*, *Volume 9. Elsevier, Amsterdam,* , 51–90.
Shannon, M., and C. Agee (1998), Percolation of core melts at lower mantle conditions, *Science*, *280*(5366), 1059-1061.
Shi, C. Y., L. Zhang, W. Yang, Y. Liu, J. Wang, Y. Meng, J. C. Andrews, and W. L. Mao (2013), Formation of an interconnected network of iron melt at Earth's lower mantle conditions, *Nature Geoscience*, *6*(11), 971.
Solomatov, V., R. El-Khozondar, and V. Tikare (2002), Grain size in the lower mantle: constraints from numerical modeling of grain growth in two-phase systems, *Physics of the Earth and planetary interiors*, *129*(3-4), 265-282.
Stevenson, D. (1990), Fluid dynamics of core formation, In: Origin of the earth. Oxford University Press , New York.
Takafuji, N., K. Hirose, S. Ono, F. Xu, M. Mitome, and Y. Bando (2004), Segregation of core melts by permeable flow in the lower mantle, *Earth and Planetary Science Letters*, *224*(3-4), 249-257.
Terasaki, H., D. J. Frost, D. C. Rubie, and F. Langenhorst (2007), Interconnectivity of Fe–O–S liquid in polycrystalline silicate perovskite at lower mantle conditions, *Physics of the Earth and Planetary Interiors*, *161*(3-4), 170-176.
Terasaki, H., T. Kato, S. Urakawa, K.-i. Funakoshi, A. Suzuki, T. Okada, M. Maeda, J. Sato, T. Kubo, and S. Kasai (2001), The effect of temperature, pressure, and sulfur content on viscosity of the Fe–FeS melt, *Earth and Planetary Science Letters*, *190*(1-2), 93-101.
Todd, K. A., H. C. Watson, T. Yu, and Y. Wang (2016), The effects of shear deformation on planetesimal core segregation: Results from in-situ X-ray micro-tomography, *American Mineralogist*, *101*(9), 1996-2004.
Tonks, W. B., and H. J. Melosh (1992), Core formation by giant impacts, *Icarus*, *100*(2), 326-346.
Tsujino, N., Y. Nishihara, D. Yamazaki, Y. Seto, Y. Higo, and E. Takahashi (2016), Mantle dynamics inferred from the crystallographic preferred orientation of bridgmanite, *Nature*, *539*(7627), 81-84.
Turcotte, D. L., and G. Schubert (2002), Geodynamics, 2nd ed, *Cambridge Univ. Press, New York*, 456.
von Bargen, N., and H. S. Waff (1986), Permeabilities, interfacial areas and curvatures of partially molten systems: results of numerical computations of equilibrium microstructures, *Journal of Geophysical Research: Solid Earth*, *91*(B9), 9261-9276.
Walte, N., D. Rubie, P. Bons, and D. Frost (2011), Deformation of a crystalline aggregate with a small percentage of high-dihedral-angle liquid: Implications for core–mantle differentiation during planetary formation, *Earth and Planetary Science Letters*, *305*(1-2), 124-134.
Yamazaki, D., T. Kato, E. Ohtani, and M. Toriumi (1996), Grain growth rates of MgSiO3 perovskite and periclase under lower mantle conditions, *Science*, *274*(5295), 2052-2054.
Zhang, Z., S. M. Dorfman, J. Labidi, S. Zhang, M. Li, M. Manga, L. Stixrude, W. F. McDonough, and Q. Williams (2016), Primordial metallic melt in the deep mantle, *Geophysical Research Letters*, *43*(8), 3693-3699.

Figure 1. Secondary electron images show the melt texture of undeformed(a) and deformed sample(b)The melts exhibit as isolated pockets in undeformed sample while are elongated in the deformed sample. Both Pt containing and Pt free melts exist in the deformed sample.

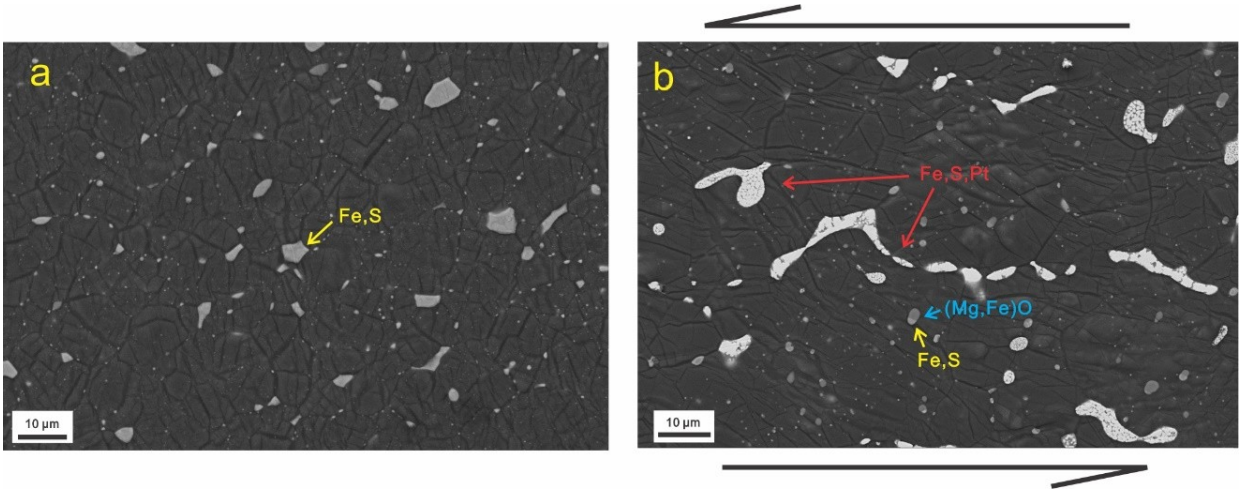

Figure 2. Backscattered electron images of undeformed(a) and deformed samples (b) and corresponding Pt mappings (c) and (d). Pt totally migrates into the Fe,S melts in the deformed sample while only partly into the Fe,S melts in undeformed sample.

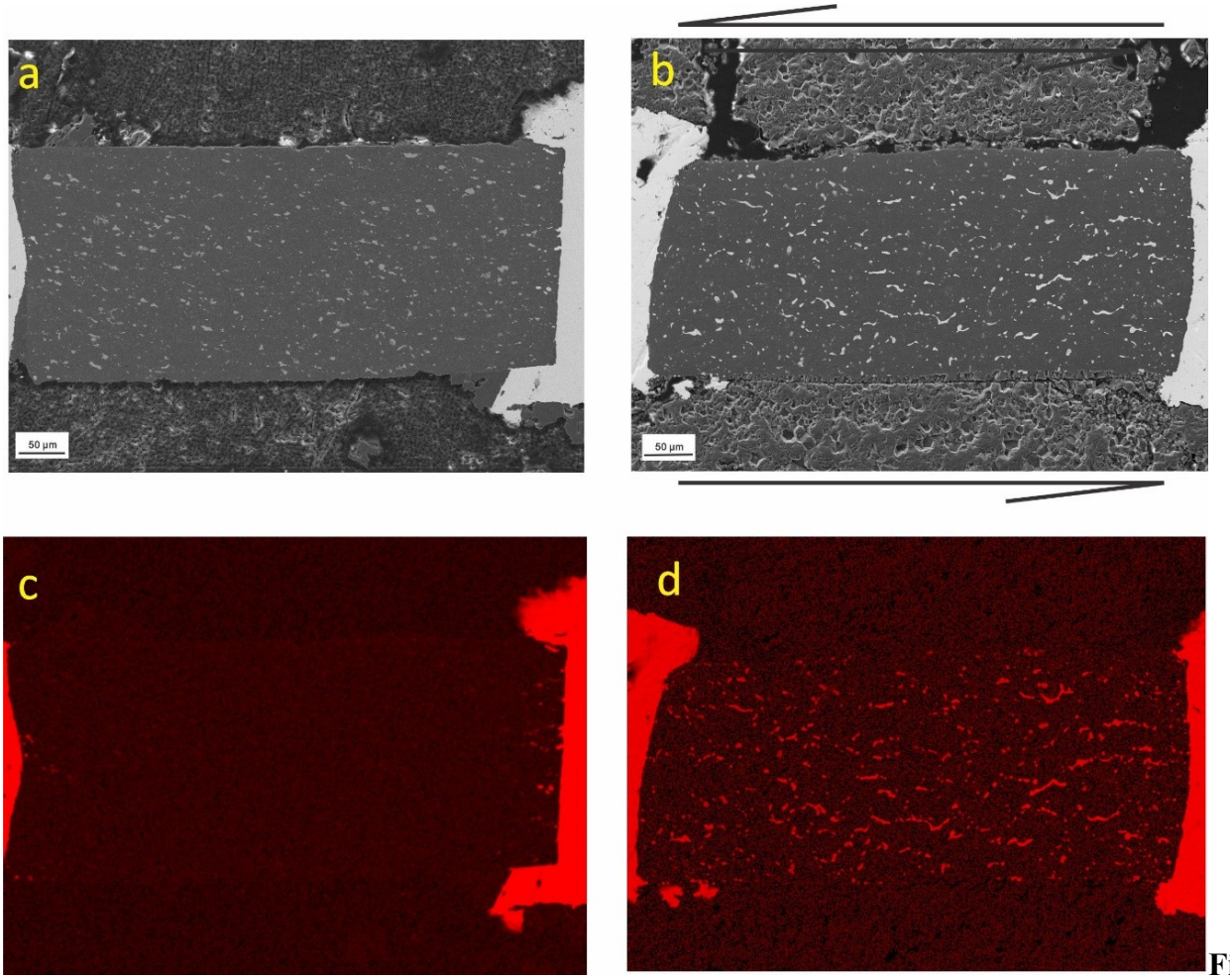

Figure 3. Segregation velocity (V_m) as function of grain size and melt fraction in the tubules model (a) and olivine-ref model (b). Contours with different V_m are shown with numbers. The blue line indicates the boundary where $d = d_s$, above which mantle is disequilibrium with the core forming melts. $d_s \sim\sqrt{Dt}$, where D is the diffusion coefficient and t is the melts residence time, which equals to the mantle thickness divided by V_m. The calculation uses D ~10^{-18} [*Holzapfel et al.*, 2005]. t is the time melt needs to travel through a 3000 km thick lower mantle.

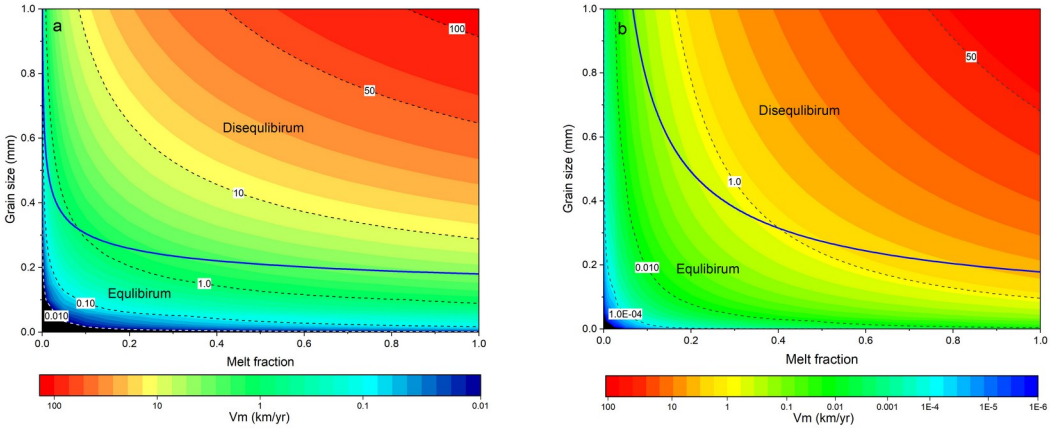
a
100
50
10
1.0
0.10
0.010
Disequlibirum
Equlibirum
Grain size (mm)
Melt fraction
Vm (km/yr)
b
50
1.0
0.010
1.0E-04
Disequlibirum
Equlibirum
Grain size (mm)
Melt fraction
Vm (km/yr)

Figure 4. Schematic diagram showing possible scenarios for the stress-induced percolation during core formation. The mantle convection and the high stress caused by the diapir descent could redistribute the core forming melts into an interconnected network. The stranded melts in the mantle could explain its chondritic abundance of HSE.